Bias correction of satellite and reanalysis products for daily rainfall occurrence and intensity

John Bagiliko [1a,b], David Stern[c], Francis Feehi Torgbor[d], Danny Parsons[a,b,c], Samuel Owusu Ansah[e], Denis Ndanguza[a]

[a] *Department of Mathematics, School of Science, College of Science and Technology, University of Rwanda , P.O. Box 3900, Kigali, Rwanda*
[b] *African Institute for Mathematical Sciences, Research and Innovation Center, Rue KG590 ST, Kigali, Rwanda*
[c] *IDEMS International, RG2 7AX, Reading, United Kingdom*
[d] *Ghana Innovations in Development, Education and the Mathematical Sciences, Okponglo, East Legon, Accra, Ghana*
[e] *Ghana Meteorological Agency, P.O. Box LG 87, Accra, Ghana*

Abstract

Study region: Ghana and Zambia, Africa

Study focus: This study rigorously evaluates a suite of bias correction (BC) methods, including statistical approaches (LOCI, QM), machine learning (SVR, GPR), and hybrid techniques (LOCI-GPR, QM-GPR), applied to seven satellite rainfall estimates (SREs) across 38 stations in Ghana and Zambia, aiming to assess their performance in rainfall detection and intensity estimation.

New hydrological insights for the region: Results indicate that the ENACTS product, which uniquely integrates a large number of station records, was the most corrigible SRE; in Zambia, nearly all BC methods successfully reduced the mean error in daily rainfall amounts at over 70% of stations. However, this performance requires further validation at independent stations not incorporated into the ENACTS product. Overall, statistical methods (QM and LOCI) generally outperformed other techniques, although QM exhibited a tendency to inflate rainfall values. All SREs corrected with the statistical and hybrid BC methods demonstrated high capability for detecting dry days (POD $\geq$ 0.80). A critical limitation persisted, however, as all SREs (except ENACTS), after correction with BC methods, consistently

[1]Corresponding author. E-mail address: john.bagiliko@aims-senegal.org

failed to improve the detection of heavy and violent rainfall events (POD $\leq$ 0.2), highlighting a crucial area for future research.

Keywords: Bias correction, Downscaling, Rainfall, Precipitation, Satellite Estimates, Africa

1. Introduction

In data-sparse regions with limited rain gauge coverage, SREs serve as an important complementary data source. These products deliver precipitation information at fine spatial and temporal scales, typically with near-global coverage.

However, SREs are known to be associated with different shortcomings, such as overestimation of rain day frequency (eg. Maphugwi et al. (2024)), overestimation or underestimation of rainfall intensities at different geographical areas, and challenge in detecting extreme rainfall events at various locations (eg. Ageet et al. (2022); Mekonnen et al. (2023)). These shortcomings could be due to indirect measurement techniques, dependence on secondary variables, and potential flaws in temporal coverage, spatial resolution, retrieval algorithms, or sensor precision, reducing their dependability for climate-related analyses (Dinku et al., 2018; Toté et al., 2015; Ayehu et al., 2018). Consequently, bias correction (BC) remains an essential step to enhance the utility of SREs for climate applications.

Numerous studies have explored traditional statistical BC techniques to improve SRE accuracy (Zhang et al., 2022; Enayati et al., 2020; Abera et al., 2016; Schmidli et al., 2006; Gudmundsson et al., 2012; Atiah et al., 2023; Nigussie et al., 2022; Katiraie-Boroujerdy et al., 2020; Mendez et al., 2020; Lakew, 2020; Shen et al., 2021; Chaudhary and C. T., 2019; Dehaghani et al., 2023; Lober et al., 2023; Asilevi et al., 2024). Traditional methods fall into two broad categories: mean-based, such as Local Intensity Scaling (LOCI), which adjust long-term averages to match gauge observations, and distribution-based methods, such as Quantile Mapping (QM), which align the statistical distributions of SREs with ground data (Soo et al., 2019). Many works have found QM and other distribution-based method to outperform other traditional statistical methods under multiple contexts for precipitation correction (Waongo et al., 2024; Lakew, 2020). However, a known limitation of this method is its tendency to inflate values (Maraun, 2013). Some recent studies have leveraged ML algorithms (Tao et al., 2016; Chen et al.,

2010; Li et al., 2023; Baez-Villanueva et al., 2020; Le et al., 2023; Tripathi et al., 2006), which all demonstrate a potential for reducing biases in SREs. Some methods specifically correct both rain day frequency and rainfall intensity. For example, LOCI and QM adjust both rain or no rain days and rainfall intensities (Maraun, 2013). In the context of bias correction, the ML approaches are generally regression-based, or a combination of classification and regression. The regression-based ML methods only correct the rainfall intensity. Others attempt to correct both rain day frequency and rainfall intensity with ML. For example, Chen et al. (2010) demonstrated an approach where numerous meteorological variables were used to first develop a rain or no-rain classifier, followed by regression models applied exclusively to wet days. Based on the notion that satellite precipitation inversion errors vary with intensity, Li et al. (2023) developed regression models (specifically Gaussian Process Regression) for different rainfall intensity classes (i.e. $0-0.1$, $0.1-10$, $10-25$, $25-50$, $50-100$, and >100 mm/day) which demonstrated good performance.

Performance of BC methods seem to depend on SRE, temporal scale, and location. Dhawan et al. (2024) compared statistical methods (Linear scaling, Variance scaling, Power transformation, QM, Multivariate bias correction) and ML methods (Decision tree regressor, Extreme gradient boosting, Support Vector Regression (SVR)) for bias-correcting ERA5-Land in two provinces of Italy, and found that the statistical methods outperformed the ML methods across monthly and daily time scales, while the ML methods had the best performance on hourly time scale. They also noted the performance of their BC methods declined from coarser temporal scales (monthly) to finer, more granular temporal scales (hourly).

Despite these efforts, comparative evaluations of BC methods remain limited for Africa (including our study area), particularly for newer SREs such as the Precipitation Estimation from Remotely Sensed Information using Artificial Neural Networks-Climate Data Record (PERSIANN-CDR, denoted PCDR) (Ashouri et al., 2015), and Enhancing National Climate Services (ENACTS) (Dinku et al., 2017, 2022). This gap is critical, given the continent's diverse climatic regimes and high reliance on rainfall for agriculture.

It is worth noting that the ENACTS rainfall product is distinct in its methodology, directly merging extensive daily station observations with bias-corrected CHIRPS (Climate Hazards Group Infrared Precipitation with Stations) or TAMSAT (Tropical Application of Meteorology using Satellite data) satellite estimates (Dinku et al., 2022). This contrasts with CHIRPS, which

incorporates station data only on a 5-day basis without full historical integration (Funk et al., 2015), and TAMSAT, which uses station data purely for calibration rather than direct merging (Maidment et al., 2017).

This study evaluated the performance of four BC methods (LOCI, QM, SVR and GPR) applied to seven SREs across 38 stations in Ghana and Zambia. The uncorrected SREs were also validated alongside. The BC methods were chosen to include both mean-, distribution-, and ML-based approaches. In addition, we also tested the potential of hybrid approaches by combining statistical methods with ML techniques: 1. LOCI-GPR (GPR applied to LOCI-corrected estimates), and 2. QM-GPR (GPR applied to QM-corrected estimates). These two hybrid approaches were compared to the four BC methods which may offer new BC options to the climate data community. For all our ML methods, we built separate models for different precipitation intensity classes (except days which SREs estimate as dry (i.e. < 0.85 mm/day)). The study region cover three major African rainfall regimes (Bagiliko et al., 2025), enabling a robust assessment of method efficacy under varying climatic conditions. Statistical evaluation metrics employed include Mean Error (ME), Correlation Coefficient (Corr), Ratio of Standard Deviations (RSD), Root Mean Squared Error (RMSE), Mean Absolute Error (MAE), the Nash-Sutcliffe efficiency (NSE), and Probability of Detection (POD) aimed at assessing various aspects of the corrected estimates with respect to the gauge data as well as the uncorrected SRE estimates.

This paper is arranged as follows: Section 2 describes the study area and data, presents the BC methods as well as the evaluation metrics; Section 3 presents the results; and Section 4 presents the discussion while the conclusion is given in Section 5.

2. Materials and methods

2.1. Study area and data

This study area comprises Zambia and Ghana (Figure 1). Ghana has two rainfall regimes (unimodal in the Savana zone, and bimodal in the Forest and Coastal zones) while Zambia has a unimodal rainfall regime. For details about climatology of these countries, refer to Jain (2007); Kaczan et al. (2013); Maidment et al. (2017); Hachigonta et al. (2008); Oduro et al. (2024); Boateng et al. (2021); Amekudzi et al. (2015); Torgbor et al. (2018); Bessah et al. (2022); Atiah et al. (2020) and Chisanga et al. (2023).

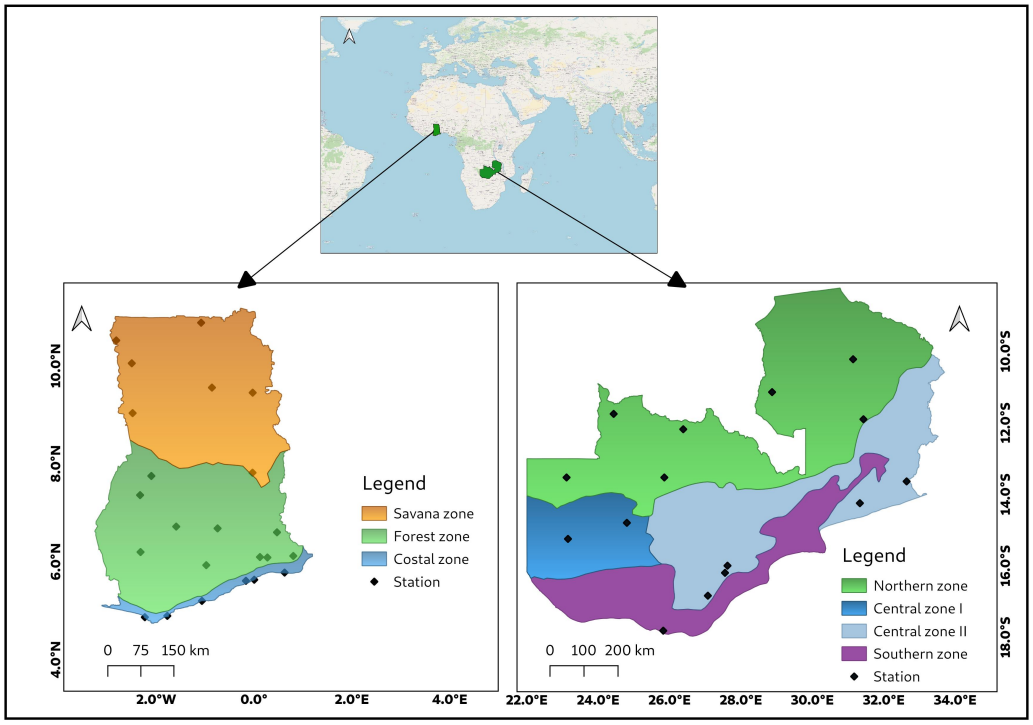

Figure 1: Map of the study area showing Ghana's climatic zones (bottom left) adapted from Bessah et al. (2022), and Zambia's agroecological zones (bottom right)

We used rain gauge data from 38 stations and processed pixel-to-point extracted SRE data. The station data, previously quality-controlled by Bagiliko et al. (2025), spans three major African rainfall regimes. These stations are distributed across both countries (23 in Ghana and 15 in Zambia), covering all the climatic and agroecological zones in Ghana and Zambia, respectively (see Figure 1).

The seven SREs were TAMSAT (Maidment et al., 2017; Tarnavsky et al., 2014; Hersbach et al., 2020), the European Centre for Medium-Range Weather Forecasts (ECMWF) v5 (ERA5) (Hersbach et al., 2020; Bell et al., 2021), the Climate Hazards Group Infrared Precipitation (CHIRP), CHIRP with Stations (CHIRPS) (Funk et al., 2014, 2015), fifth-generation reanalysis of ECMWF (AgERA5 referred here as AGERA5) (Boogaard et al., 2020; Copernicus Climate Change Service, 2019), PCDR (Ashouri et al., 2015), and ENACTS (Dinku et al., 2017, 2022). These SREs uniformly possess long historical records ($>$ 30 years), high spatial resolution (a minimum of 0.25°),

and fine temporal resolution (daily and sub-daily), while also encompassing Africa or portions of the study region (see Table 1).

Table 1: Details of SREs used in the study

Product	**Coverage**	**Period**	**Resolution**	**Reference**
CHIRPS	Global	1981–present	0.05° daily	Funk et al. (2014, 2015)
CHIRP	Global	1981–present	0.05° daily	Funk et al. (2014, 2015)
TAMSAT	Africa	1983–present	0.0375° daily	Maidment et al. (2017), Tarnavsky et al. (2014), Hersbach et al. (2020)
ERA5	Global	1940–present	0.25° hourly	Bell et al. (2021) Hersbach et al. (2020)
AGERA5	Global	1979–present	0.1° daily	Boogaard et al. (2020)
ENACTS	Selected countries	1981–present	0.0375° daily	Dinku et al. (2017, 2022)
PCDR	Global	1983–present	0.25° daily	Ashouri et al. (2015)

2.2. Bias correction methods

This study evaluates a comprehensive suite of BC methods: LOCI, QM, SVR, GPR. The methods were chosen to cover mean-based (LOCI), distribution-based (QM), and ML-based approaches (SVR and GPR). In addition, we also tested the potential of hybrid approaches by combining conventional methods with ML techniques: 1. LOCI-GPR (GPR applied to LOCI-corrected estimates), and 2. QM-GPR (GPR applied to QM-corrected estimates).

For each BC method, the models were trained (or fitted) using historical data spanning 1983 to 2000. Subsequently, these trained models were tested on data from 2001 to 2022, or for the full available data length (see Figure 2). The period 1983-2000 was used for the training to ensure we had enough training data.

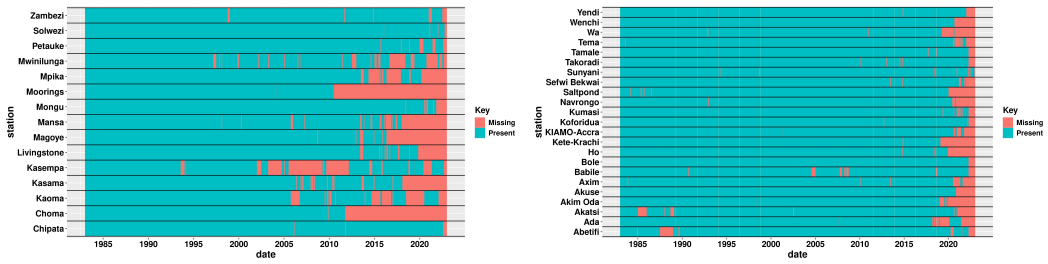

(a) (b)

Figure 2: Inventory plot of the station data used in the study for both Zambia (a) and Ghana (b)

Our approach hinges on the assumption that mean rainfall characteristics remain relatively similar between the training (1983-2000) and test (2001-2022) periods. We acknowledge that this assumption might be challenged by potential climate change effects, which could alter rainfall patterns over time. Some previous works have also used this approach (Li et al., 2023; Dhawan et al., 2024). A key advantage of our chosen temporal split strategy is its utility for infilling missing data within the test period. Since our models only require SRE data and the fitted function (model), they can readily estimate missing gauge observations in the testing period. At each station, distinct models were developed (fitted) for each SRE, ensuring tailored corrections.

An alternative strategy, often adopted in other studies, involves training models at one station and testing them on a neighboring station. However, this "spatial transferability" approach has its limitations, particularly if training and test stations are geographically distant or lack similar climatological characteristics. Given the significant distances between our study stations, this spatial transfer approach may not be suitable for our context. Stations are sparsely located in many African countries, so this approach would be less applicable in other similar contexts.

The BC methods are presented as follows:

2.2.1. LOCI

LOCI (Schmidli et al., 2006) first calculates a scale factor, defined in (1).

$$s_m = \frac{mean(x_i | x_i \geq T_m^x) - T_m^x}{mean(y_i | y_i \geq T_m^y) - T_m^y}, \tag{1}$$

where x_i is the station rainfall value on day i in month m, y_i is SRE rainfall value on day i in month m, T_m^y is the rain day threshold of the SRE in month

m, with rain day threshold $T_m^x = 0.85$ (STERN and COOPER, 2011).

The threshold T_m^y was obtained through quantile matching:

$$T_m^y = F_{y_m}^{-1}\left(F_{x_m}(T_m^x)\right) \tag{2}$$

where F_{x_m} is the Empirical cumulative distribution function (CDF) of station rainfall in month m, F_{y_m} is the empirical CDF of SRE rainfall in month m, and $F_{y_m}^{-1}$ is the inverse CDF of SRE rainfall.

This ensures equivalent wet-day probabilities:

$$P(y_i \geq T_m^y) = P(x_i \geq T_m^x) \tag{3}$$

Finally, the scale factor is used to obtain y_i', the bias-corrected SRE rainfall value on day i given in (4).

$$y_i' = \begin{cases} 0, & \text{if } y_i \leq T_m^y \\ T_m^x + s_m(y_i - T_m^y), & \text{otherwise} \end{cases} \tag{4}$$

2.2.2. QM

The QM method aligns the probability distribution of the rainfall values from the SRE with the distribution of the observed data (Gudmundsson et al., 2012). This is achieved by ensuring that the cumulative distribution function (CDF) of SRE data and observed data are consistent (Gudmundsson et al., 2012). The rain day frequency was first adjusted with T_m^y obtained in Section 2.2.1. Gamma cumulative distribution functions were then fitted to both the SRE data and corresponding station data. The bias-corrected daily rainfall estimates of the SRE data were obtained by using the inverse CDF of the observed data as shown in (5).

$$P_{bc} = F_o^{-1}(F_{SRE}(P_{SRE})), \tag{5}$$

where P_{bc} is the bias-corrected daily rainfall values of the SRE, $F_o^{-1}()$ is the inverse CDF of P_o (the observed data) known as the quantile function (Enayati et al., 2020), and $F_{SRE}()$ is the CDF of the SRE data (P_{SRE}).

2.2.3. GPR

A Gaussian Process (GP) is defined by a mean function $m(x)$ and a covariance function $k(x, x')$, for inputs x and x' (Rasmussen and Williams, 2006; Schulz et al., 2018). Given a training dataset $\mathbf{X}$ consisting of input

vectors x_i and their corresponding target values y_i, and a test set $\mathbf{X}_*$ for which we want to predict the corresponding outputs f_*, the joint distribution of the observed target values $\mathbf{y}$ and the function values $\mathbf{f}_*$ at the test points under the Gaussian Process (GP) prior is given by:

$$\begin{pmatrix} \mathbf{y} \\ \mathbf{f}_* \end{pmatrix} \sim \mathcal{N}\left(\mathbf{0}, \begin{bmatrix} K(\mathbf{X},\mathbf{X}) + \sigma_n^2 I & K(\mathbf{X},\mathbf{X}_*) \\ K(\mathbf{X}_*,\mathbf{X}) & K(\mathbf{X}_*,\mathbf{X}_*) \end{bmatrix}\right) \tag{6}$$

where $K(\mathbf{X},\mathbf{X})$ is the covariance matrix computed with the kernel function k for all pairs of training points, $K(\mathbf{X},\mathbf{X}_*)$ is the covariance matrix between the training points and the test points, $K(\mathbf{X}_*,\mathbf{X}_*)$ is the covariance matrix for the test points, σ_n^2 represents the noise variance in the observations, and I is the identity matrix.

Given this joint distribution, the conditional distribution of the function values $\mathbf{f}_*$ at the test points given the observed data $\mathbf{y}$, the posterior distribution, is:

$$\mathbf{f}_*|\mathbf{X},\mathbf{y},\mathbf{X}_* \sim \mathcal{N}(\boldsymbol{\mu}_*, \Sigma_*) \tag{7}$$

where the posterior mean $\boldsymbol{\mu}_*$ and covariance Σ_* are given by:

$$\boldsymbol{\mu}_* = K(\mathbf{X}_*,\mathbf{X})[K(\mathbf{X},\mathbf{X}) + \sigma_n^2 I]^{-1}\mathbf{y} \tag{8}$$

$$\Sigma_* = K(\mathbf{X}_*,\mathbf{X}_*) - K(\mathbf{X}_*,\mathbf{X})[K(\mathbf{X},\mathbf{X}) + \sigma_n^2 I]^{-1}K(\mathbf{X},\mathbf{X}_*) \tag{9}$$

In our context, $\mathbf{X}$ contains two vectors: the daily SRE estimates at a given station, and the SRE values of the previous day used during training; $\mathbf{y}$ represents the daily rainfall observations at a corresponding station used during training; and $\mathbf{X}_*$ contains the daily SRE estimates at same station as well as the SRE values of the previous day used during testing. We used the Matérn kernel given by:

$$k(x,x') = \sigma^2 \frac{2^{1-\nu}}{\Gamma(\nu)} \left(\frac{\sqrt{2\nu}d}{\rho}\right)^{\nu} K_\nu \left(\frac{\sqrt{2\nu}d}{\rho}\right) \tag{10}$$

where $k(x,x')$ is the covariance function, σ^2 is the variance parameter, ν is a parameter that controls the smoothness of the kernel, $\Gamma(\nu)$ is the gamma function, ρ is the length scale parameter, $d = \|x - x'\|$, and K_ν is the modified Bessel function of the second kind of order ν.

Different GPR models were built for different rainfall intensity categories (i.e. [0.85, 5), [5, 20), [20, 40), and > 40 mm/day), and the rainfall values were also normalized as done by Li et al. (2023).

2.2.4. SVR

SVR is a supervised ML technique based on Support Vector Machines initially developed by Vapnik and Chervonenkis in 1963 (Cortes and Vapnik, 1995; García-Floriano et al., 2018). The prediction function for SVR is given by:

$$f(x) = \sum_{i=1}^{n} (\alpha_i - \alpha_i^*) k(x_i, x) + b \tag{11}$$

where α_i and α_i^* are Lagrange multipliers obtained from the optimization process (Schölkopf et al., 2000), $k(x_i, x)$ is the kernel function evaluating the similarity between a new data point x and the support vectors x_i, n is the number of support vectors, and b is the bias term. The radial basis function $k(x_i, x)$ defined in (12) was used.

$$k(x, x') = v^2 \exp\left(-\frac{\|x - x'\|^2}{2\lambda^2}\right) \tag{12}$$

where x, x' are vectors in the input space, v^2 is the kernel variance, $\|x - x'\|$ is the Euclidean distance between the vectors x and x', and λ is the length scale parameter, which determines the smoothness of the function.

Training the SVR means:

$$\min_{w,b,\xi,\xi^*} \left(\frac{1}{2}\|w\|^2 + C\sum_{i=1}^{n}(\xi_i + \xi_i^*)\right) \tag{13}$$

subject to the following constraints:

$$y_i - (w^T\phi(x_i) + b) \leq \epsilon + \xi_i, \tag{14}$$

$$(w^T\phi(x_i) + b) - y_i \leq \epsilon + \xi_i^*, \tag{15}$$

$$\xi_i, \xi_i^* \geq 0 \quad \forall i. \tag{16}$$

where w is the weight vector, ξ and ξ^* are the slack variables, $\phi(x_i)$ represents the feature mapping of x_i, and C is the regularization parameter controlling the trade-off between the flatness of the model and the amount up to which deviations larger than ϵ are tolerated.

As in the case of GPR, the rainfall data was normalized and different SVR models were trained for different rainfall intensity categories.

2.2.5. LOCI-GPR and QM-GPR

The initial step involved deriving the LOCI scale factor, given in (1), and the QM quantile function, given in (5) from the 1983-2000 training data. These were then applied to correct daily SRE values throughout the entire 1983-2022 period. This full-period correction was crucial to ensure that the subsequent training (1983-2000) and test (2001-2022) subsets maintained consistent statistical properties.

Following this, GPR (presented in Section 2.2.3) was trained and evaluated separately. One GPR model used the LOCI-corrected data (divided into its own training and test periods) giving the LOCI-GPR model, and another used the QM-corrected data (also split into training and test periods) producing the QM-GPR model.

The rainfall values were also normalized, and different GPR models were built for different rainfall intensity categories.

2.3. Evaluation metrics

We evaluated the effectiveness of the BC methods on the SREs in capturing rainfall occurrence and intensity using independent test data. The assessment employed six complementary statistical metrics: Mean Error (ME), Pearson's correlation coefficient (Corr), Ratio of Standard Deviations (RSD), Root Mean Squared Error (RMSE), Mean Absolute Error (MAE), Nash-Sutcliffe efficiency (NSE) for both daily and annual scales. Probability of Detection (POD) was additionally used for evaluation at the daily temporal scale for assessing the ability of the SREs to detect dry days, heavy and violent rainfall events. These metrics collectively assess different dimensions of agreement between the corrected estimates, original SREs, and ground-based gauge observations. ME measures the average model bias, where positive and negative values signify systematic overestimation and underestimation of observed rainfall, respectively (Enyew et al., 2024). The Corr quantifies the strength and direction of the linear relationship between the estimates and observations, ranging from -1 to 1 (Yang et al., 2016). A value approaching $+1$ denotes a strong ability to capture temporal rainfall variability. RSD compares the variability of the estimates to the observations. An RSD value of 1 indicates perfect agreement, values >1 suggest over-dispersion, and values <1 indicate under-dispersion. The POD assesses the likelihood that a rainfall event identified by the gauge is also correctly detected by the SRE or its corrected version. The NSE is a normalized statistic that evaluates

predictive skill. An NSE of 1 represents a perfect model, a value of 0 indicates predictions are as accurate as the mean of the observations, and values significantly below 0 suggest poor model performance. The RMSE is measure of error magnitude that is sensitive to large outliers due to the squaring of terms. A perfect score is 0. Finally, MAE provides a direct measure of average error magnitude and is less sensitive to extreme values than RMSE. Table 2 provides a summary of the metrics used in the evaluation.

Table 2: Statistical metrics used for BC evaluation

Metric	**Formula**	**Range**	**Optimal Value**
ME	$\frac{1}{n}\sum_{i=1}^{n}(P_i - O_i)$	$(-\infty, +\infty)$	0
Corr	$\frac{\sum(P_i-\bar{P})(O_i-\bar{O})}{\sqrt{\sum(P_i-\bar{P})^2\sum(O_i-\bar{O})^2}}$	[-1, 1]	1
RSD	σ_P/σ_O	$(0, +\infty)$	1
RMSE	$\sqrt{\frac{1}{n}\sum_{i=1}^{n}(P_i - O_i)^2}$	$[0, +\infty)$	0
MAE	$\frac{1}{n}\sum_{i=1}^{n}\lvert P_i - O_i\rvert$	$[0, +\infty)$	0
NSE	$1 - \frac{\sum(P_i-O_i)^2}{\sum(O_i-\bar{O})^2}$	$(-\infty, 1]$	1
POD	$\frac{\text{Hits}}{\text{Hits+Misses}}$	[0, 1]	1

P_i: predicted value; O_i: observed value; $\bar{P}, \bar{O}$: means of predicted and observed values respectively; σ_P, σ_O: standard deviations of predicted and observed values respectively; n: sample size; Hits: correct rainfall events detected; Misses: undetected rainfall events; False Alarms: rainfall event predicted but not observed.

3. Results

This section presents the study's results at daily, seasonal, and annual scales.

3.1. Performance of BC methods on daily scale

3.1.1. Overall performance of BC methods and SREs on daily rainfall amounts

The efficacy of the BC methods was evaluated by their ability to reduce mean error (ME) in the SREs. Bubble plots in Figures 3(a) and (b) display the proportion of stations in Zambia and Ghana, respectively, where a given BC method (y-axis) reduced the daily ME relative to the uncorrected SRE (x-axis). Bubble color represents the mean RSD across these stations, while bubble size corresponds to the proportion of stations. The mean RSD is also

displayed numerically within each bubble. Missing bubbles indicate BC-SRE combinations that yielded no improvement.

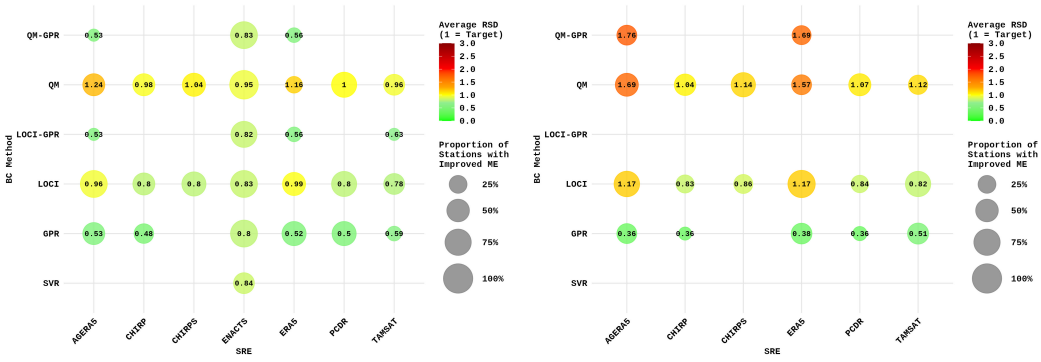

(a) (b)

Figure 3: Bubble plots evaluating BC method performance in reducing ME on daily rainfall amounts for Zambia (a) and Ghana (b). Each bubble's position shows a BC method and SRE combination, its size shows the proportion of stations with reduced ME, and its colour shows the mean RSD at those stations. Missing bubbles indicate no improvement

Figure 3(a) revealed that the efficacy of the BC methods in Zambia varied substantially by SRE and station. When applied to ENACTS, almost all BC methods reduced the ME at a high proportion of stations (>70%). Among them, QM and LOCI were particularly effective, successfully reducing ME for most SREs across many stations while maintaining reasonable variability (RSD close to 1), underscoring their superiority for capturing daily rainfall amounts.

In contrast, GPR reduced MEs for some stations across all SREs except CHIRPS. Analysis of daily values indicated that GPR typically underestimated rainfall, leading to negative MEs and lower variability. This suggests GPR is most effective at stations where the uncorrected SREs had high positive biases. This explains its poor performance with CHIRPS and TAMSAT, which generally exhibited low positive or negative biases (Figure S1), as GPR's underestimation worsened their MEs. This tendency to underestimate was even more pronounced for SVR and the hybrid methods QM-GPR and LOCI-GPR, resulting in a substantial reduction of variability (RSD ≤ 0.63) as seen in Figure 3(a).

The strong performance of BC methods on ENACTS is likely a character-

istic of the ENACTS dataset itself, rather than the BC methods. Although uncorrected ENACTS had a negative ME, methods like GPR, SVR, and the hybrids still reduced this error, contrary to their behavior with other SREs, indicating that the initial distribution of ENACTS is more amenable to these corrections.

A similar pattern was observed in Ghana (Figure 3(b)), where QM and LOCI again improved ME at many stations while preserving reasonable variability. However, for the reanalysis products (AGERA5 and ERA5), which had high positive uncorrected MEs (Figure S2), QM significantly overestimated variability. GPR's performance in Ghana was similar to that in Zambia, reducing ME for all SREs except CHIRPS. SVR and LOCI-GPR failed to improve ME at any station in Ghana, while the hybrid QM-GPR only showed improvement for AGERA5 and ERA5, albeit with overestimated variability.

The previous indicator, based solely on the reduction of ME, can be noisy, as a reported reduction or increase in ME might be negligible in magnitude. To reduce the effect of this noise, we introduced another indicator: whether the BC method brings the ME within an acceptable threshold, defined as less than 20% of the observed mean daily rainfall. This indicator identifies substantial improvements together with minor, inconsequential changes (i.e. slight decrease or increase in ME).

Figures 4(a) and (b) present bubble plots showing the proportion of stations in Zambia and Ghana, respectively, where the BC methods achieved an acceptable ME. In these plots, bubble sizes represent the proportion of stations, while bubble colours show the corresponding average RSD, with the mean RSD value displayed numerically inside each bubble.

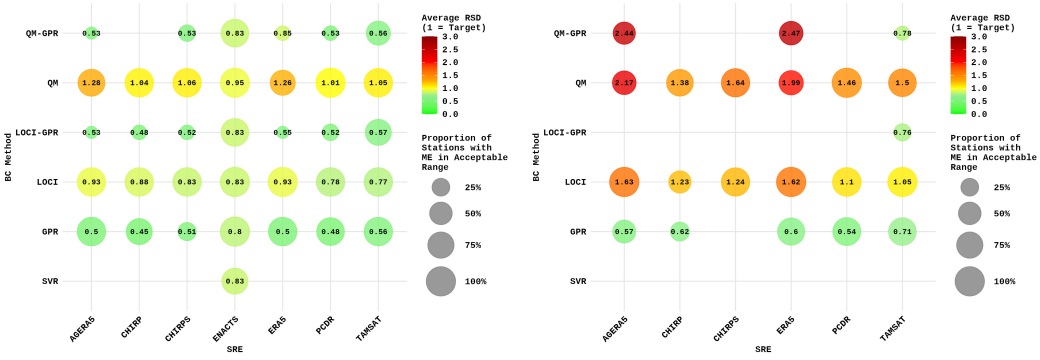

(a) (b)

Figure 4: Proportion of stations in Zambia (a) and Ghana (b) where BC methods achieved an acceptable ME ($<$ 20% of observed mean rainfall). Bubble sizes correspond to the proportion of stations; colours indicate the mean RSD (also displayed inside the bubbles)

In Zambia (Figure 4(a)), QM and LOCI consistently produced acceptable MEs at nearly all stations for all SREs, while also maintaining realistic variability (RSD close to 1), although QM overestimated variability for AGERA5 and ERA5. GPR also achieved acceptable MEs for most SREs except CHIRPS, for which it often performed poorly. This, along with its characteristically low variability across most SREs, is consistent with its tendency to underestimate rainfall. The hybrid methods (LOCI-GPR and QM-GPR) and SVR resulted in acceptable MEs at only a few stations, which aligns with their previously observed underestimating behaviour. ENACTS stood out as the SRE for which all BC methods achieved acceptable MEs at nearly all stations with reasonable variability. This robust performance appears to be an inherent property of the ENACTS dataset itself, as it even persisted with methods like LOCI-GPR, QM-GPR, and SVR, which otherwise performed poorly.

In Ghana (Figure 4(b)), LOCI and QM produced acceptable MEs at a high proportion of stations for all SREs. However, QM tended to highly overestimate variability, an effect particularly pronounced for AGERA5 and ERA5 whose uncorrected versions mostly underestimated rainfall (negative MEs), had low correlations and low variability. The overestimation in variability by QM on these SREs is likely due to the introduction of high rainfall values on wrong days, leading to high positive biases and reduced correlations (Table S1). GPR, LOCI-GPR, and SVR consistently underestimated

rainfall, resulting in MEs outside the acceptable range for most SREs. Conversely, QM-GPR performed consistently across SREs, except for AGERA5 and ERA5, where it overestimated variability, a behaviour likely attributable to the intrinsic properties of these reanalysis SREs.

3.1.2. Detection of dry days

All the SREs in their uncorrected form already showed high POD for dry days (POD $>$ 0.7) across all stations in Zambia. This high detection rate can be seen in Figure 5, a map comparing the performance of the various BCs to uncorrected CHIRP, faceted by the methods. It was also the case for CHIRPS and TAMSAT in Ghana (CHIRPS shown in Figure 6). For these cases LOCI, LOCI-GPR, QM, QM-GPR all still increased the POD slightly further improving the detection of dry days, while SVR and GPR did not show observable changes. The improvement of the detection of dry days is not surprising since they specifically adjusted the number of rainy days. There is, however, a risk of missing some rainy days.

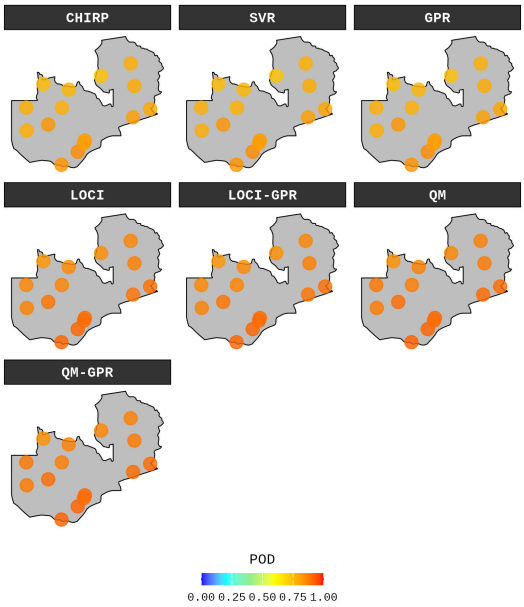

Figure 5: Probability of Detection (POD) of dry days by the BC methods on CHIRP across different stations in Zambia

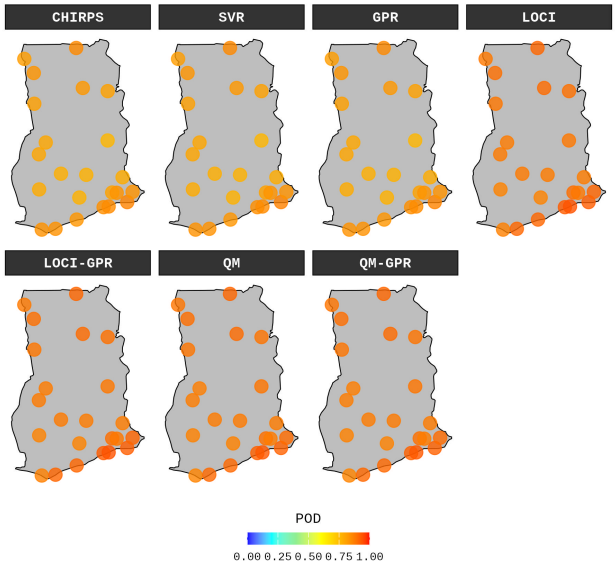

Figure 6: POD of dry days by the BC methods on CHIRPS across different stations in Ghana

For ERA5, AGERA5, PCDR, and CHIRP in Ghana, the detection of dry days by their uncorrected versions was quite poor in the Forest and Coastal zones (southen part of the country) while their performance in the Savannah zone (northern part) is comparable to the performance of CHIRPS and TAMSAT. Figures 7(a) and 7(b) show the perfomance of the BC methods applied to ERA5 and CHIRP, respectively, compared to the uncorrected versions of these SREs for the detection of dry days across the stations in Ghana. As expected LOCI, LOCI-GPR, QM, QM-GPR slightly improved the detection of dry days in the Savannah zone, and significantly increased the POD in the Forest and Coastal zones. There was no observable improvement by SVR and GPR, which is also expected.

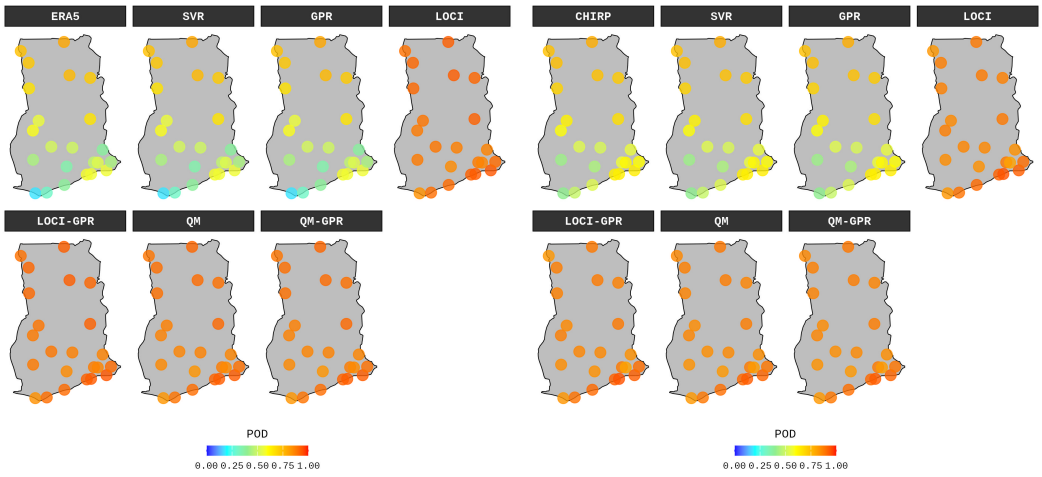

(a) (b)

Figure 7: POD on the detection dry days by the BC methods when applied on ERA5 (a) and CHIRP (b) across different stations in Ghana

3.1.3. Detection of heavy rains

All SREs in their uncorrected form demonstrated poor detection of heavy rains $25 \leq \text{rain} < 40$) across Ghana and Zambia (with POD < 0.2) at most stations. SVR, GPR, LOCI-GPR and QM-GPR applied on the SREs (with the exception of ENACTS) further worsen their ability to detect this rainfall event in both Ghana and Zambia due to their tendency to underestimate the daily rainfall amounts. LOCI and QM seemed to slightly improve the POD. This trend can be seen in Figures 8 and 9. Figure 8 shows the performance of the BCs applied to CHIRPS compared to its uncorrected version across the stations in Ghana while Figure 9 shows the performance of the BCs applied to PCDR compared to its uncorrected version across the stations in Zambia. The improvement by LOCI and QM were only slight increases in the POD, which generally still remained below 0.20 in both Zambia and Ghana.

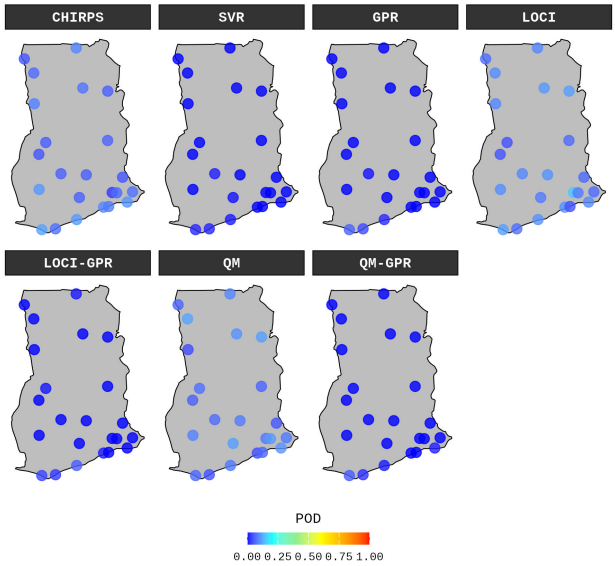

Figure 8: POD of heavy rains by the BC methods on CHIRPS across different stations in Ghana

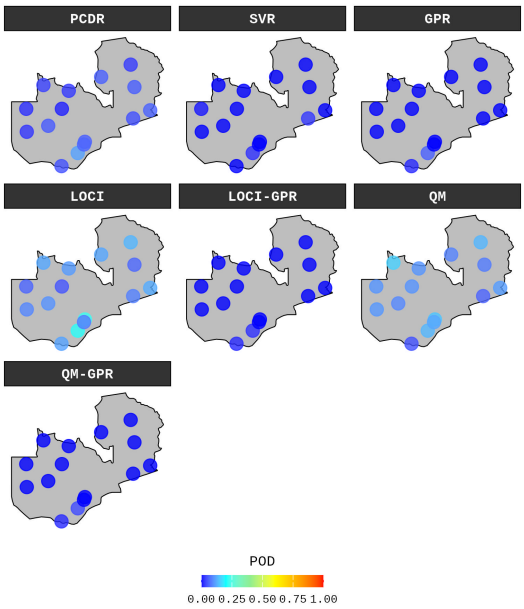

Figure 9: POD of heavy rains by the BC methods on PCDR across different stations in Zambia

ENACTS, on the other hand, showed quite a different behavior when the BCs were applied on it. All BCs seemed to increase the POD (see Figure 10) at most stations indicating an improved capability to detect heavy rainfall in Zambia.

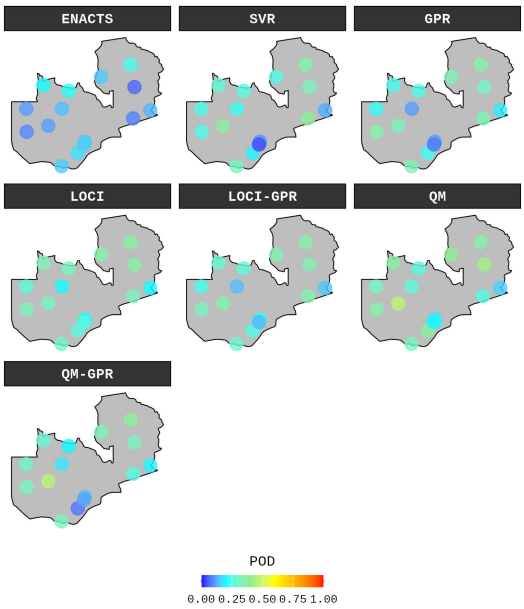

Figure 10: POD of heavy rains by the BC methods on ENACTS across different stations in Zambia

Tables 3 presents the performance of the QM method on ENACTS for detecting heavy rainfall events in Zambia. The QM-corrected ENACTS showed improved POD across all stations, though the magnitude of improvement varied. Some stations experienced substantial increases, for example, Mongu saw POD rise from 0.092 to 0.354, while Moorings had only marginal gains (0.157 to 0.196). Notably, stations with the lowest initial POD in uncorrected ENACTS exhibited the most significant improvements after QM correction.

Similar enhancements were observed across Zambia for other BCs applied to ENACTS, though their impact was generally smaller than that of QM (as can be seen in Figure 10). However, there were observable reduction reduction in POD at few stations by SVR, GPR, LOCI-GPR, and QM-GPR. One of these few stations happened to be Moorings, where the four BC methods all worsened the POD compared to the uncorrected ENACTS.

Table 3: Performance comparison of ENACTS and QM-corrected ENACTS (QM) for Heavy rain detection. Under Event Counts, the values under ENACTS and QM are the total model predictions (25-40 mm), combining true and false positives, while Observed is the total number of observed heavy rain events ($25 \leq \text{rain} < 40$)

Station	POD		Event Counts		
	ENACTS	QM	Observed	ENACTS	QM
Chipata	0.132	0.159	153	116	119
Choma	0.170	0.377	53	53	101
Kaoma	0.112	0.469	99	53	135
Kasama	0.233	0.360	150	141	200
Kasempa	0.140	0.262	107	102	207
Livingstone	0.157	0.314	70	49	76
Magoye	0.148	0.182	88	68	100
Mansa	0.151	0.397	126	106	182
Mongu	0.092	0.354	132	66	155
Moorings	0.157	0.196	51	62	123
Mpika	0.063	0.429	112	54	174
Mwinilunga	0.204	0.369	157	129	225
Petauke	0.085	0.254	119	45	128
Solwezi	0.213	0.255	193	130	210
Zambezi	0.111	0.309	166	83	144

3.1.4. Detection of violent rains

All the SREs in their uncorrected form had very low POD (close to 0) for the detection of violent rains ($\geq$ 40 mm/day) at almost every station in Ghana and Zambia. The BCs applied on the SREs (except ENACTS) produced only slight increases or decreases in POD, which generally remained below 0.20. LOCI and QM tended to slightly increase the POD in most cases for the SREs in Zambia, with QM showing the most increase (as can be seen in Figure 11, which shows the performance of the BCs applied to TAMSAT compared to its uncorrected version across the stations). Similar observations were made for the SREs in Ghana except for AGERA5 and ERA5, where QM-GPR also showed slight increase in POD at many of the stations, even though POD still generally remained below 0.20 (see Figure 12, which shows the performance of the BC methods applied to AGERA5 compared to its uncorrected version across the stations in Ghana).

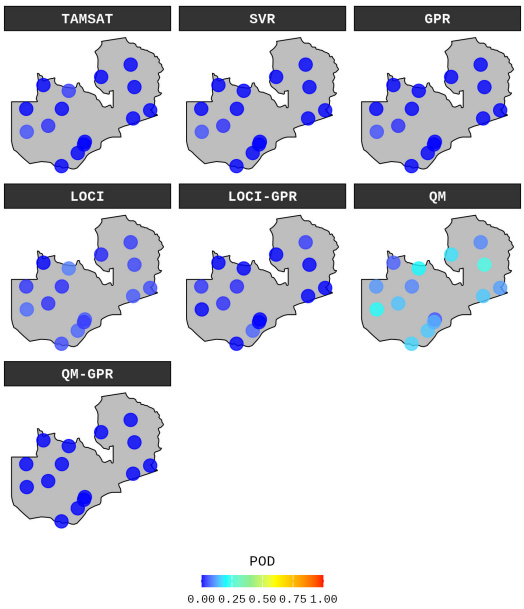

Figure 11: POD of violent rains by the BC methods on TAMSAT across different stations in Zambia

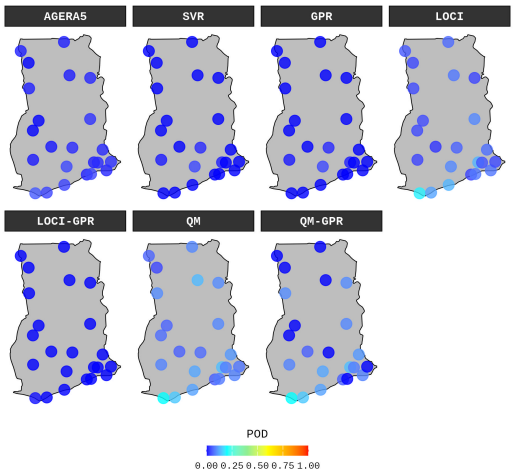

Figure 12: POD of violent rains by the BC methods on AGERA5 across different stations in Ghana

All the BC methods applied on ENACTS seemed to improve the POD

for the detection of violent rains (with POD > 0.2 at almost all stations). QM showed the most improvement (see Figure 13) at most stations.

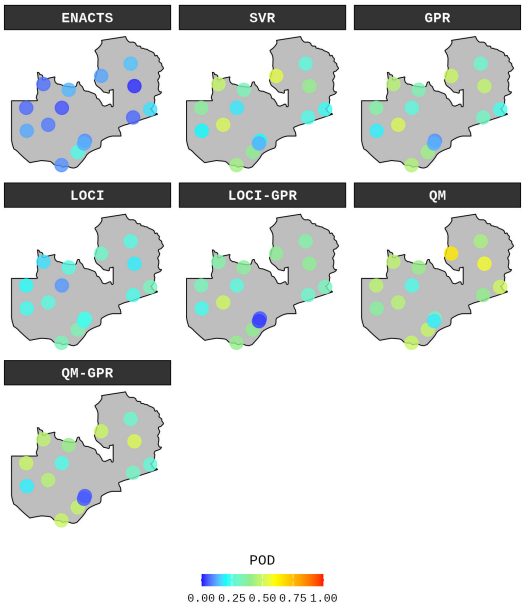

Figure 13: POD of violent rains by the BC methods on ENACTS across different stations in Zambia

Table 4 compares the performance of the QM method against uncorrected ENACTS for detecting violent rainfall events in Zambia. The QM correction substantially improved the POD across all stations except Moorings. Notably, at Chipata, Mansa, and Mpika, the POD exceeded 0.50 after correction, a substantial increase from their initial values of 0.173, 0.118, and 0.017, respectively. In contrast, Moorings saw only a marginal improvement ($+0.051$) from its baseline POD of 0.128.

Table 4: Performance comparison of ENACTS and QM-corrected ENACTS for violent rain detection. Under Event Counts, the values for ENACTS and QM are the total model predictions (≥ 40), combining true and false positives, while Observed is the total actual violent rain events (rain ≥ 40)

Station	POD		Event Counts		
	ENACTS	QM	Observed	ENACTS	QM
Chipata	0.173	**0.503**	179	34	125
Choma	0.242	0.485	33	10	36
Kaoma	0.080	0.460	50	5	31
Kasama	0.145	0.434	76	18	63
Kasempa	0.045	0.242	66	4	30
Livingstone	0.102	0.490	49	5	31
Magoye	0.098	0.317	41	11	38
Mansa	0.118	**0.647**	85	11	84
Mongu	0.121	0.374	91	18	68
Moorings	0.128	0.179	39	12	38
Mpika	0.017	**0.576**	59	1	61
Mwinilunga	0.069	0.471	87	7	69
Petauke	0.063	0.405	79	5	62
Solwezi	0.135	0.413	104	15	85
Zambezi	0.067	0.467	90	7	68

3.2. Performance of the BC methods on seasonal scale

To model daily rainfall occurrence, a Zero-Order Markov chain approach was used. The probability of rainfall occurrence for each day of the year was derived using logistic regression, which incorporated Fourier series terms to account for cyclical seasonal patterns. The analysis was restricted to days where concurrent data were available from all sources (gauge observations, SREs, and BC outputs) to guarantee a consistent temporal comparison.

Figures 14 through 17 were generated using an identical methodology. In these figures, the observed rain day frequency from gauge data, using a 0.85 mm threshold, is represented by a solid black curve. The corresponding frequency from the SRE data is depicted by a solid red curve. The results from the various BC methods are illustrated by coloured dashed curves. The y-axis indicates the proportion of rain days, and the x-axis represents the date, ranging from August 1 to July 31 for Zambia and from January 1 to December 31 for Ghana.

In general, QM, QM-GPR, LOCI and LOCI-GPR applied on the SREs all captured the seasonality well at the various stations (have similar dome shapes as the gauge curve in solid black line) both in Ghana and Zambia (Figures 14 15, 16, and 17) and aligned with the gauge proportion of rainy days at most stations, especially for Zambia. This is expected as these methods do not specifically adjusted the rain day frequency.

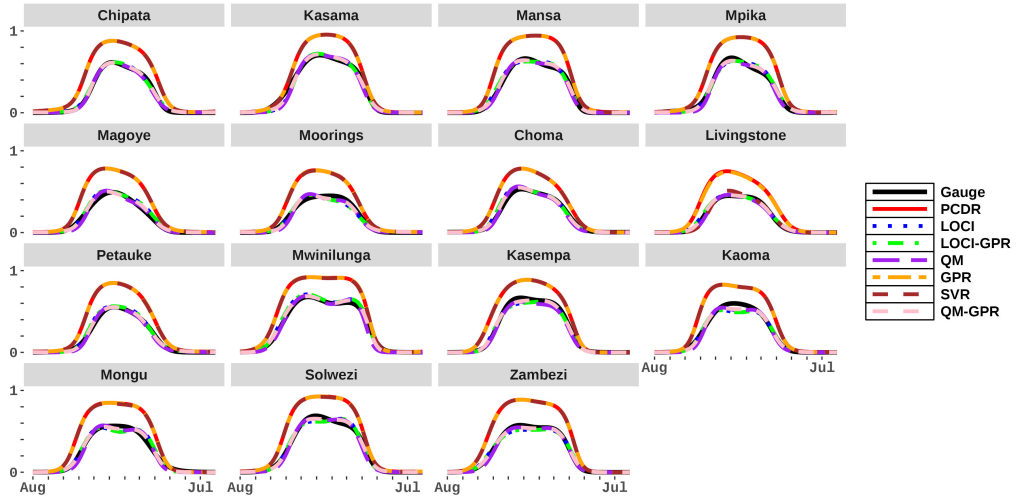

Figure 14: Performance of the BC methods on PCDR for capturing rainfall seasonality across the stations in Zambia. The y-axis represents the probability of rain, while the x-axis represents the day of year (starting August and ending July)

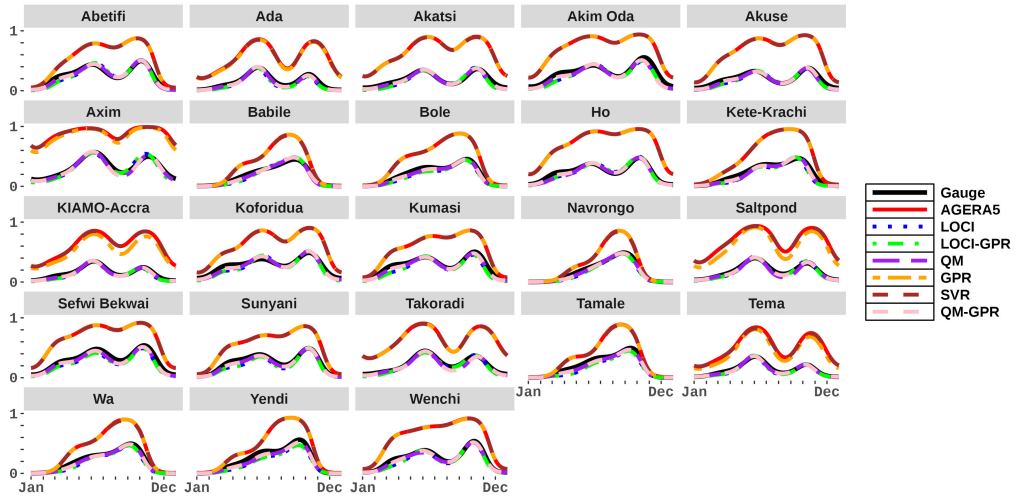

Figure 15: Performance of the BC methods on AGERA5 for capturing rainfall seasonality across the stations in Ghana. The y-axis represents the probability of rain, while the x-axis represents the day of year (January - December)

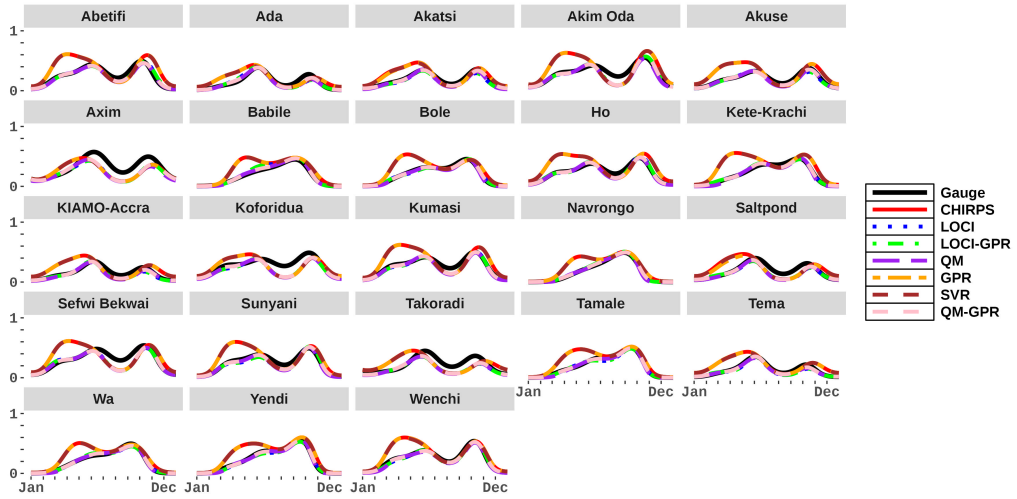

Figure 16: Performance of the BC methods on CHIRPS for capturing rainfall seasonality across the stations in Ghana. The y-axis represents the probability of rain, while the x-axis represents the day of year (January - December)

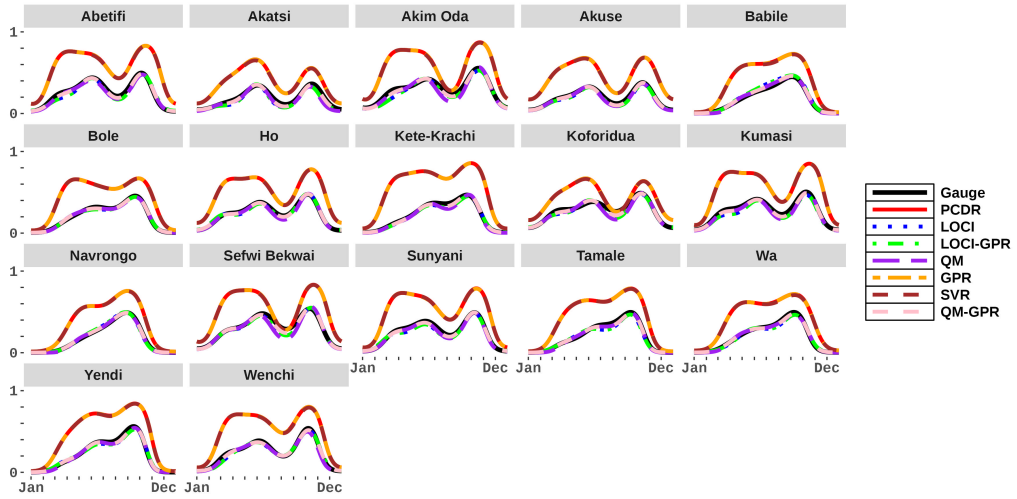

Figure 17: Performance of the BC methods on PCDR for capturing rainfall seasonality across the stations in Ghana. The y-axis represents the probability of rain, while the x-axis represents the day of year (January - December)

As expected, SVR- and GPR-corrected SREs still aligned with seasonal patterns of the uncorrected SREs (see Figures 14, 15, 16, and 17), which all tended to overestimate the proportion of rain at different times of the year. This is is due to the fact that they do not specifically adjust the rain day frequency.

At some of the stations in Ghana, the rainfall regime (bi-modal or uni-modal) did not seem to be captured by the uncorrected SREs as well as their SVR- and GPR-corrected versions. For example, Figure 15 shows the performance of the BC methods on AGERA5 for capturing rainfall seasonality across the stations in Ghana. In this figure, the uncorrected AGERA5 as well as its SVR- and GPR-corrected versions did not clearly show a bimodal rainfall pattern at some of the stations in the Forest zone such as Kumasi, Sunyani and Wenchi as it is for the observed data and the other BC methods. Also, Figure 17 shows the performance of the BC methods on PCDR for capturing rainfall seasonality across the stations in Ghana. The uncorrected PCDR as well as its SVR- and GPR-corrected versions did not seem to clearly depict a unimodal rainfall pattern at some of the stations in the Savanna zone such as Bole.

Persistent underestimations were observed in CHIRPS rain day proportions at some coastal and southern stations, particularly between the dual

peaks of the rainy seasons (Figure 16). These systematic biases remained uncorrected by all the BC methods. Similar underestimation patterns were evident in TAMSAT data for a couple of stations in the Forest and Coastal zones (see Figure S14 in supplementary material).

3.3. Performance of the BC methods on annual scale

3.3.1. Number of rainy days

Tables 5 and 6 show the overall MEs on number of rainy days by SRE and BC method across all stations in Zambia and Ghana, respectively. All uncorrected SREs overestimated the annual number of rainy days (positive MEs) in both countries. In Zambia, ENACTS had the lowest bias (+9.224 days), followed by CHIRPS (+13.931 days), while the remaining SREs exhibited substantial overestimates, ranging from over 22 to 55 days, as shown in Table 5. QM ended up with underestimates between 1 to 6 days for some SREs. The cause of this was largely due to the application of a slightly higher rain day threshold (estimated from the training period) to the test period (Figure S16 in supplementary material).

LOCI, LOCI-GPR, QM, and QM-GPR all significantly reduced these biases. SVR and GPR did not substantially change the number of rainy days across the SREs, which is tied to the fact the that they do not specifically adjust the number of rainy days.

Table 5: Overall Mean Errors by SRE and BC method across the stations in Zambia

SRE	**Uncorrected**	**LOCI**	**LOCI-GPR**	**QM**	**GPR**	**SVR**	**QM-GPR**
CHIRPS	13.931	3.356	3.356	−2.236	13.902	13.632	1.546
CHIRP	51.966	10.460	10.454	0.374	51.966	50.983	3.920
ERA5	56.299	−0.845	−0.845	−3.966	55.397	55.914	−0.667
TAMSAT	22.925	2.827	2.827	−5.214	22.925	22.699	0.486
ENACTS	9.224	3.800	3.800	−3.812	9.188	4.624	1.527
PCDR	51.770	1.453	1.453	−2.205	51.658	48.385	1.118
AGERA5	55.391	−0.063	−0.069	−4.425	54.500	55.069	−0.626

In Ghana, the overestimation by the uncorrected SREs was more pronounced. The SREs with the largest biases were ERA5 (+134.111 days) and AGERA5 (+122.246 days), while CHIRPS had the smallest overestimation (+23.527 days), see Table 6. However, they tended to underestimate the

rainy days up to 10 days, due to a slightly higher rain day threshold from the training period applied to the test period that should have lesser threshold (Figure S15 in Supplementary Material). As expected, SVR and GPR only slightly reduced the MEs across all SREs.

Table 6: Overall Mean Errors by SRE and BC method across the stations in Ghana

SRE	**Uncorrected**	**LOCI**	**LOCI-GPR**	**QM**	**GPR**	**SVR**	**QM-GPR**
CHIRPS	23.527	−8.891	−8.908	−10.556	23.191	22.806	−7.844
CHIRP	99.939	−5.067	−5.081	−5.106	99.664	98.662	−2.087
AGERA5	122.246	−10.794	−10.853	−7.028	117.570	121.530	−6.388
ERA5	134.111	−9.811	−9.847	−6.081	126.373	133.323	−4.903
PCDR	90.057	−5.029	−5.032	−5.271	90.019	89.334	−2.481
TAMSAT	55.314	1.193	1.181	−4.767	55.186	54.705	−0.458

At station level, the performance of the uncorrected SREs exhibited a north-south gradient in Ghana. Apart from CHIRPS and TAMSAT, the SREs showed a higher overestimation of the number of rainy days in the southern parts of the country (Forest and Coastal Zones) as compared to northern stations (Savannah zone). For these SREs, LOCI, LOCI-GPR, QM, and QM-GPR reduced the biases, aligning closely with the observed number of rainy days across all stations, while SVR and GPR did not show any substantial changes, as expected.

For instance, Figure 18(a) shows the MEs for the BC methods applied to AGERA5 for the annual number of rainy days across different stations in Ghana. In this figure, the north-south variation in overestimation is visible for the uncorrected AGERA5. The LOCI-, LOCI-GPR-, QM-, and QM-GPR-corrected versions of AGERA5 drastically reduced the biases.

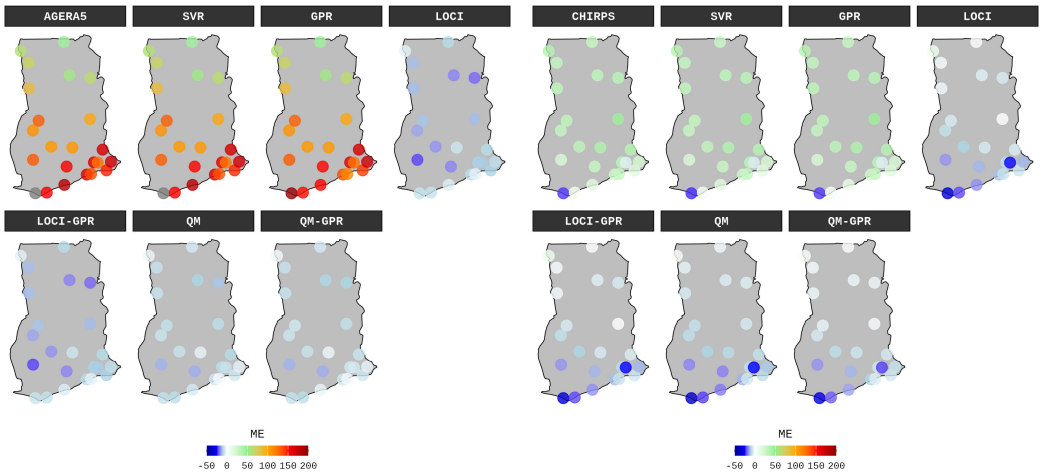

(a) (b)

Figure 18: Mean Error (ME) on the annual number of rainy days across different stations in Ghana when the BC methods were applied on AGERA5 (a) and CHIRPS (b)

In contrast, CHIRPS and TAMSAT showed a higher overestimation of the number of rainy days in the Savanna and Forest zones of the country. These overestimations were less pronounced in the far Coastal areas than in the northern locations in Ghana (Figure 18(b), and Figure S6 respectively).

LOCI, QM, LOCI-GPR, and QM-GPR reduced the biases, aligning closely with the observed number of rainy days at most stations in Ghana and Zambia. However these same BC methods methods tended to cause slight underestimations in both Ghana and Zambia, even though it was lower for Zambia (Figures 18, and Figures S3-S13) due to the rain day threshold shift between training period and test period (Figures S15 and S16 in supplementary material).

3.3.2. Mean rain per rainy day

In this section the interest was to assess the performance of the BC methods on mean rain per rainy day, i.e, the total amount of rain in a year divided by the number of rainy days in the year. The BC methods was evaluated by their ability to reduce mean error (ME) in the SREs as well as improve variability.

Bubble plots in Figures 19(a) and (b) display the proportion of stations in Zambia and Ghana, respectively, where a given BC method (y-axis) reduced

the ME relative to the uncorrected SRE (x-axis). Bubble color represents the mean RSD across these stations, while bubble size corresponds to the proportion of stations. The mean RSD is also displayed numerically within each bubble. Missing bubbles indicate BC-SRE combinations that yielded no improvement.

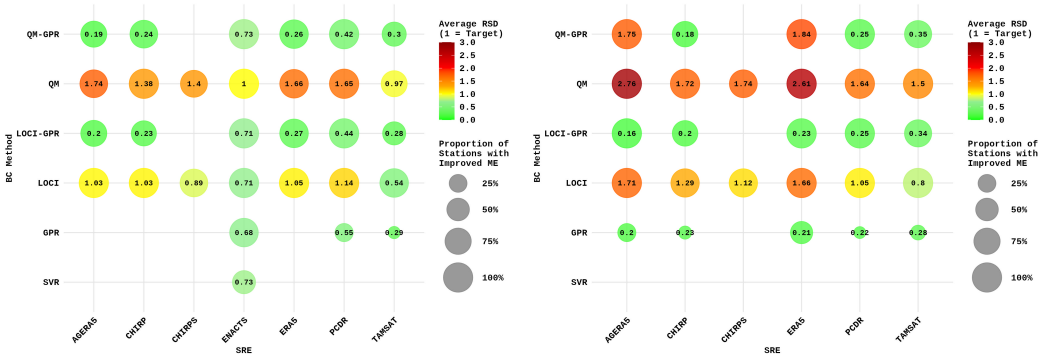

(a) (b)

Figure 19: Bubble plots evaluating BC method performance in reducing ME on mean rain per rainy day for Zambia (a) and Ghana (b). Each bubble's position shows a BC method and SRE combination, its size shows the proportion of stations with reduced ME, and its color shows the mean RSD at those stations, also displayed inside the bubbles. Missing bubbles indicate no improvement

From Figure 19(a) LOCI and QM reduced the MEs for the mean rain per rainy day at almost all stations in Zambia for all SREs. This is expected as these BC methods reduced the systematic overestimation in number of rainy days observed for almost all the uncorrected SREs (Table 5) while the corrected daily amounts where within acceptable range with the observed daily rainfall (Figure 4(a)). LOCI tended to have RSD closer to 1 for almost all SREs, signifying a similar variability with observed mean rain per rainy day. QM tended to overestimate the variability across all SREs. This is likely due to the introduction of high values not observed. LOCI-GPR and QM-GPR also reduced the ME at most of the stations for almost all SREs, except CHIRPS. This is explained by the correction in number of rainy days (closer to observed number of rainy days) and reduced MEs in the daily rainfall amounts. The low low variability in the many cases is as a result of the less variable bias-corrected daily values leading to flat totals. There were

less instances where GPR improved the MEs (apart from ENACTS), which is expected as it underestimated the rainfall amounts while it did not correct the overestimation in the number of rainy days. Apart from ENACTS, SVR did not improve ME for any SRE at any station, also explained by similar behaviour as GPR but with higher underestimation in the rainfall amounts. ENACTS stood out as the product where all SREs reduced the MEs, which as a result of the SREs having low MEs on the daily rainfall amounts while all having closer number of rainy days as the observed data (see Table 5).

The trends observed in the performance of the BCs for capturing mean rain per rainy day in Ghana (Figure 19(b)) were not very different, in most cases, from those observed in Zambia. The most obvious difference was in the magnitude of the RSD, especially for QM which tended to highly overestimate the variability for all SREs, especially for AGERA5 and ERA5. LOCI and QM-GPR also overestimated variability for those two SREs. This is likely as a result of the introduction of high values on wrong days while they have their number of rain days closer to the observed.

4. Discussion

This study offers new insights into the performance of a comprehensive suite of BC methods, including ML, statistical, and hybrid approaches, applied to a wide range of SREs across diverse climates in Ghana and Zambia. It identifies key nuances in both the SREs and BC methods that lead to their success or failure in detecting rainfall occurrence and estimating intensity. Furthermore, the study highlights how external factors like location and regional characteristics influence the bias correction process.

ENACTS is generated by merging extensive ground station observations with bias-corrected CHIRPS or TAMSAT data (Dinku et al., 2022). This contrasts with CHIRPS, which incorporates station data only on a five-day basis without full historical integration (Funk et al., 2015), and TAMSAT, which uses station data purely for calibration rather than direct merging (Maidment et al., 2017). ENACTS was the standout SRE in Zambia, with all BC methods performing well across multiple contexts. For example, nearly all the BC methods applied to ENACTS reduced the mean error (ME) at over 70% of stations in Zambia (Figure 3(a)), even when the same methods substantially increased errors for other SREs. The efficacy of BC methods on ENACTS is likely due to the comprehensive integration of station data within the product. For instance, nearly all BC methods applied to ENACTS

enhanced the detection of heavy and violent rainfall events across almost all stations (Tables 3 and 4), except at Moorings, where most BC methods decreased the probability of detection. This station was likely not included in ENACTS. The performance at locations not included in this SRE therefore requires further investigation. The Zambia Meteorological Department is preparing data from volunteer stations not currently in ENACTS; whilst not yet available, these data could serve as a basis for a follow-up study.

SREs are known to struggle with the accurate detection of heavy and violent rainfall events (Yang et al., 2016; Mekonnen et al., 2023; Zambrano-Bigiarini et al., 2017; Ageet et al., 2022). This challenge, as recent work by Li et al. (2023) has shown, often persists even after BC. Our results corroborate this, indicating that, with the notable exception of ENACTS (which needs further investigation), the applied BC methods did not significantly improve SREs' ability to detect these events. Future work should specifically target these extreme events. Chen et al. (2010) demonstrated an approach where numerous meteorological variables were used to first develop a rain or no-rain classifier, followed by regression models applied exclusively to wet days. Building upon this, future research could focus on creating models specifically designed to identify heavy and violent rainfall days. Subsequently, regression models could be applied to these classified events to bias-correct their intensities. Existing research already shows promise in classifying such events. Yang and Villarini (2019) investigated the temporal clustering of heavy precipitation events in Europe using reanalysis datasets, revealing that these events indeed exhibit clustering patterns that reanalysis products effectively reproduce. The inclusion of diverse meteorological variables, similar to those in these studies, will likely provide strong signals for successfully classifying these critical events.

QM, along with other distribution-based techniques, has consistently demonstrated superior performance over other traditional statistical methods in various contexts of precipitation correction (Waongo et al., 2024; Lakew, 2020). This advantage is largely attributed to QM's ability to maintain the full statistical distribution of rainfall as well as the long term means, while simultaneously addressing both intensity and rain day frequency biases (Maraun, 2013). Furthermore, some studies have shown that QM and other statistical methods can outperform ML approaches (Dhawan et al., 2024). In line with these findings, the statistical methods in our study generally outperformed the ML approaches. However, a known limitation of QM is its tendency to inflate rainfall values (Maraun, 2013), which was evident in our

results, where QM-corrected SREs often overestimated rainfall amounts and increased variability relative to station observations.

In contrast to our findings, Li et al. (2023), who performed BC on IMERG-FR data over the Guangdong-Hong Kong-Macao Greater Bay Area, reported that ML methods (GPR and SVR) outperformed statical QM method. This discrepancy underscores that the performance of BC methods depends on various factors, including location, the SRE used, and regional characteristics. The length of data records may also be a factor; Li et al. (2023) acknowledged that the short historical record used to establish their transfer function might have limited QM's applicability during testing.

The topography of southern Ghana (encompassing Forest and Coastal zones) is complex due to its vegetation, terrain, and proximity to the coast. These regions experience highly localized rainfall events (Amekudzi et al., 2015), which SREs struggle to detect accurately. We found that uncorrected SREs underestimated rainy days at some stations, a problem that was exacerbated by the BC methods, especially in Ghana's Forest and Coastal zones (see Figure 18 and Supplementary Materials Figures S3-S12). Given the inherent limitations of point-to-pixel comparison, a slight overestimation of rainy days by SREs is not only more realistic than an underestimation, but is often the more acceptable outcome, even if perfect equality remains the ideal. Our investigation revealed that the underestimation was due to a shift in the rain-day threshold between the training period (1983–2000) and the test period (2001-2022). The thresholds derived from the training period were higher than the actual thresholds in the test period at some stations, causing some rainy days with values below these thresholds to be misclassified as dry. While the potential influence of climate change on this threshold shift cannot be ruled out, the more pronounced effect in Ghana may have resulted from noise caused by localized rainfall events that were captured differently between the two periods. In any case, the choice of training period seems to have an impact on the results for LOCI, QM, LOCI-GPR, and QM-GPR. This will be worth investigating further in future studies.

5. Conclusion

This study rigorously evaluated a comprehensive suite of bias correction (BC) methods, including statistical approaches (LOCI, QM), machine learning (SVR, GPR), and hybrid techniques (LOCI-GPR, QM-GPR), applied to seven satellite rainfall estimates (SREs) across 38 stations in Ghana and

Zambia, aiming to assess their performance in rainfall detection and intensity estimation.

The study demonstrates that BC methods can significantly enhance the utility of SREs for hydrological applications in Ghana and Zambia. The ENACTS product emerged as the most corrigible SRE, with nearly all BC methods successfully reducing mean error in daily rainfall amounts across most stations in Zambia. However, this performance requires validation at independent stations not incorporated into ENACTS.

Statistical methods (QM and LOCI) generally outperformed machine learning and hybrid approaches, though QM showed a tendency to inflate rainfall values.

All SREs corrected with QM, LOCI, LOCI-GPR, and QM-GPR exhibited strong capability for detecting dry days (POD ≥ 0.80) across all stations.

A critical limitation persists across most SREs and BC methods, with consistent failure to improve detection of heavy and violent rainfall events (POD ≤ 0.2), except with ENACTS. This represents a crucial research gap requiring further investigation.

Declarations

- **Funding** This publication was made possible by a grant from Carnegie Corporation of New York (provided through the African Institute for Mathematical Sciences). The statements made and views expressed are solely the responsibility of the author(s).

- **Competing interests** The authors have no relevant financial or non-financial interests to disclose.

- **Data Availability** The RE data used are all publicly available. The station data for Ghana and Zambia can be obtained from the Ghana Meteorological Agency, and the Zambia Meteorological Department, respectively.

- **Code availability** Code is available upon a reasonable request.

- **Authors' contributions** Conceptualization: J.B., D.S.; Methodology: J.B., D.S.; Formal analysis: J.B., D.S.; Data curation: J.B., D.S., F.F.T., D.P., S.O.A.; Writing — original draft: J.B.; Writing — review & editing: J.B., D.S., D.N., F.F.T., D.P., S.O.A.; Visualization: J.B., D.S.; Supervision: D.S., D.N., F.F.T.

References

Abera, W., Brocca, L., Rigon, R., 2016. Comparative evaluation of different satellite rainfall estimation products and bias correction in the upper blue nile (ubn) basin. Atmospheric Research 178-179, 471–483. URL: https://www.sciencedirect.com/science/article/pii/S0169809516301065, doi:https://doi.org/10.1016/j.atmosres.2016.04.017.

Ageet, S., Fink, A.H., Maranan, M., Diem, J.E., Hartter, J., Ssali, A.L., Ayabagabo, P., 2022. Validation of satellite rainfall estimates over equatorial east africa. Journal of Hydrometeorology 23, 129–151. URL: http://dx.doi.org/10.1175/JHM-D-21-0145.1, doi:10.1175/jhm-d-21-0145.1.

Amekudzi, L., Yamba, E., Preko, K., Asare, E., Aryee, J., Baidu, M., Codjoe, S., 2015. Variabilities in rainfall onset, cessation and length of rainy season for the various agro-ecological zones of ghana. Climate 3, 416–434. URL: http://dx.doi.org/10.3390/cli3020416, doi:10.3390/cli3020416.

Ashouri, H., Hsu, K.L., Sorooshian, S., Braithwaite, D.K., Knapp, K.R., Cecil, L.D., Nelson, B.R., Prat, O.P., 2015. PERSIANN-CDR: Daily precipitation climate data record from multisatellite observations for hydrological and climate studies. Bulletin of the American Meteorological Society 96, 69–83. URL: https://doi.org/10.1175/bams-d-13-00068.1, doi:10.1175/bams-d-13-00068.1.

Asilevi, P.J., Dogbey, F., Boakye, P., Aryee, J.N.A., Yamba, E.I., Owusu, S.Y., Peprah, D.K., Quansah, E., Klutse, N.A.B., Bentum, J.K., Adjei, K.A., Anornu, G.K., Oduro-Kwarteng, S., Amekudzi, L.K., 2024. Bias-corrected nasa data for aridity index estimation over tropical climates in ghana, west africa. Journal of Hydrology: Regional Studies 51, 101610. URL: https://www.sciencedirect.com/science/article/pii/S2214581823002975, doi:https://doi.org/10.1016/j.ejrh.2023.101610.

Atiah, W.A., Johnson, R., Muthoni, F.K., Mengistu, G.T., Amekudzi, L.K., Kwabena, O., Kizito, F., 2023. Bias correction and spatial disaggregation of satellite-based data for the detection of rainfall seasonality indices. Heliyon 9, e17604. URL:

https://www.sciencedirect.com/science/article/pii/S2405844023048120, doi:https://doi.org/10.1016/j.heliyon.2023.e17604.

Atiah, W.A., Mengistu Tsidu, G., Amekudzi, L.K., Yorke, C., 2020. Trends and interannual variability of extreme rainfall indices over ghana, west africa. Theor. Appl. Climatol. 140, 1393–1407.

Ayehu, G.T., Tadesse, T., Gessesse, B., Dinku, T., 2018. Validation of new satellite rainfall products over the upper blue nile basin, ethiopia. Atmospheric Measurement Techniques 11, 1921–1936. URL: https://amt.copernicus.org/articles/11/1921/2018/, doi:10.5194/amt-11-1921-2018.

Baez-Villanueva, O.M., Zambrano-Bigiarini, M., Beck, H.E., McNamara, I., Ribbe, L., Nauditt, A., Birkel, C., Verbist, K., Giraldo-Osorio, J.D., Xuan Thinh, N., 2020. Rf-mep: A novel random forest method for merging gridded precipitation products and ground-based measurements. Remote Sensing of Environment 239, 111606. URL: https://www.sciencedirect.com/science/article/pii/S0034425719306261, doi:https://doi.org/10.1016/j.rse.2019.111606.

Bagiliko, J., Stern, D., Ndanguza, D., Torgbor, F.F., 2025. Validation of satellite and reanalysis rainfall products against rain gauge observations in ghana and zambia. Theoretical and Applied Climatology 156, 241. URL: https://doi.org/10.1007/s00704-025-05462-7, doi:10.1007/s00704-025-05462-7.

Bell, B., Hersbach, H., Simmons, A., Berrisford, P., Dahlgren, P., Horányi, A., Muñoz-Sabater, J., Nicolas, J., Radu, R., Schepers, D., Soci, C., Villaume, S., Bidlot, J., Haimberger, L., Woollen, J., Buontempo, C., Thépaut, J., 2021. The era5 global reanalysis: Preliminary extension to 1950. Quarterly Journal of the Royal Meteorological Society 147, 4186–4227. URL: http://dx.doi.org/10.1002/qj.4174, doi:10.1002/qj.4174.

Bessah, E., Amponsah, W., Ansah, S.O., Afrifa, A., Yahaya, B., Wemegah, C.S., Tanu, M., Amekudzi, L.K., Agyare, W.A., 2022. Climatic zoning of ghana using selected meteorological variables for the period 1976–2018. Meteorological Applications 29. URL: http://dx.doi.org/10.1002/met.2049, doi:10.1002/met.2049.

Boateng, G., Asuah, M., Kyeremeh, E., Otoo, K., Otoo, E., 2021. Rainfall distribution over ghana: The effect of distance from the sea. International Journal of Research and Innovation in Social Science 5, 560–566.

Boogaard, H., Schubert, J., De Wit, A., Lazebnik, J., Hutjes, R., Van der Grijn, G., et al., 2020. Agrometeorological indicators from 1979 to present derived from reanalysis. Copernicus Climate Change Service (C3S) Climate Data Store (CDS) 10. doi:10.24381/cds.6c68c9bb.

Chaudhary, S., C. T., D., 2019. Investigating the performance of bias correction algorithms on satellite-based precipitation estimates, in: Neale, C.M., Maltese, A. (Eds.), Remote Sensing for Agriculture, Ecosystems, and Hydrology XXI, SPIE. p. 39. URL: http://dx.doi.org/10.1117/12.2533214, doi:10.1117/12.2533214.

Chen, S.T., Yu, P.S., Tang, Y.H., 2010. Statistical downscaling of daily precipitation using support vector machines and multivariate analysis. Journal of Hydrology 385, 13–22. URL: http://dx.doi.org/10.1016/j.jhydrol.2010.01.021, doi:10.1016/j.jhydrol.2010.01.021.

Chisanga, C.B., Nkonde, E., Phiri, E., Mubanga, K.H., Lwando, C., 2023. Trend analysis of rainfall from 1981-2022 over zambia. Heliyon 9. URL: https://doi.org/10.1016/j.heliyon.2023.e22345, doi:10.1016/j.heliyon.2023.e22345. accessed: 2025-06-03.

Copernicus Climate Change Service, 2019. Agrometeorological indicators from 1979 up to 2019 derived from reanalysis. URL: https://cds.climate.copernicus.eu/doi/10.24381/cds.6c68c9bb, doi:10.24381/CDS.6C68C9BB.

Cortes, C., Vapnik, V., 1995. Support-vector networks. Machine Learning 20, 273–297. URL: https://doi.org/10.1007/BF00994018, doi:10.1007/BF00994018.

Dehaghani, A.M., Gohari, A., Zareian, M.J., Torabi Haghighi, A., 2023. A comprehensive evaluation of the satellite precipitation products across iran. Journal of Hydrology: Regional Studies 46, 101360. URL: https://www.sciencedirect.com/science/article/pii/S2214581823000472, doi:https://doi.org/10.1016/j.ejrh.2023.101360.

Dhawan, P., Dalla Torre, D., Niazkar, M., Kaffas, K., Larcher, M., Righetti, M., Menapace, A., 2024. A comprehensive comparison of bias correction methods in climate model simulations: Application on era5-land across different temporal resolutions. Heliyon 10, e40352. URL: https://www.sciencedirect.com/science/article/pii/S2405844024163839, doi:https://doi.org/10.1016/j.heliyon.2024.e40352.

Dinku, T., Faniriantsoa, R., Cousin, R., Khomyakov, I., Vadillo, A., Hansen, J.W., Grossi, A., 2022. ENACTS: Advancing climate services across africa. Frontiers in Climate 3. URL: https://doi.org/10.3389/fclim.2021.787683, doi:10.3389/fclim.2021.787683.

Dinku, T., Funk, C., Peterson, P., Maidment, R., Tadesse, T., Gadain, H., Ceccato, P., 2018. Validation of the chirps satellite rainfall estimates over eastern africa. Quarterly Journal of the Royal Meteorological Society 144, 292–312. doi:10.1002/qj.3244.

Dinku, T., Thomson, M.C., Cousin, R., del Corral, J., Ceccato, P., Hansen, J., Connor, S.J., 2017. Enhancing national climate services (ENACTS) for development in africa. Climate and Development 10, 664–672. URL: https://doi.org/10.1080/17565529.2017.1405784, doi:10.1080/17565529.2017.1405784.

Enayati, M., Bozorg-Haddad, O., Bazrafshan, J., Hejabi, S., Chu, X., 2020. Bias correction capabilities of quantile mapping methods for rainfall and temperature variables. Journal of Water and Climate Change 12, 401–419. URL: https://doi.org/10.2166/wcc.2020.261, doi:10.2166/wcc.2020.261, arXiv:https://iwaponline.com/jwcc/article-pdf/12/2/401/865958/jwc0120401.pdf.

Enyew, F.B., Sahlu, D., Tarekegn, G.B., Hama, S., Debele, S.E., 2024. Performance evaluation of cmip6 climate model projections for precipitation and temperature in the upper blue nile basin, ethiopia. Climate 12. URL: https://www.mdpi.com/2225-1154/12/11/169, doi:10.3390/cli12110169.

Funk, C., Peterson, P., Landsfeld, M., Pedreros, D., Verdin, J., Shukla, S., Husak, G., Rowland, J., Harrison, L., Hoell, A., Michaelsen,

J., 2015. The climate hazards infrared precipitation with stations—a new environmental record for monitoring extremes. Scientific Data 2. URL: http://dx.doi.org/10.1038/sdata.2015.66, doi:10.1038/sdata.2015.66.

Funk, C.C., Peterson, P.J., Landsfeld, M.F., Pedreros, D.H., Verdin, J.P., Rowland, J.D., Romero, B.E., Husak, G.J., Michaelsen, J.C., Verdin, A.P., 2014. A quasi-global precipitation time series for drought monitoring. Data Series 832. U.S. Geological Survey. Reston, VA. URL: https://pubs.usgs.gov/publication/ds832, doi:10.3133/ds832.

García-Floriano, A., López-Martín, C., Yáñez-Márquez, C., Abran, A., 2018. Support vector regression for predicting software enhancement effort. Information and Software Technology 97, 99–109. URL: http://dx.doi.org/10.1016/j.infsof.2018.01.003, doi:10.1016/j.infsof.2018.01.003.

Gudmundsson, L., Bremnes, J.B., Haugen, J.E., Engen Skaugen, T., 2012. Technical note: Downscaling rcm precipitation to the station scale using quantile mapping – a comparison of methods URL: http://dx.doi.org/10.5194/hessd-9-6185-2012, doi:10.5194/hessd-9-6185-2012.

Hachigonta, S., Reason, C., Tadross, M., 2008. An analysis of onset date and rainy season duration over zambia. Theoretical and applied climatology 91, 229–243.

Hersbach, H., Bell, B., Berrisford, P., Hirahara, S., Horányi, A., Muñoz-Sabater, J., Nicolas, J., Peubey, C., Radu, R., Schepers, D., Simmons, A., Soci, C., Abdalla, S., Abellan, X., Balsamo, G., Bechtold, P., Biavati, G., Bidlot, J., Bonavita, M., Chiara, G., Dahlgren, P., Dee, D., Diamantakis, M., Dragani, R., Flemming, J., Forbes, R., Fuentes, M., Geer, A., Haimberger, L., Healy, S., Hogan, R.J., Hólm, E., Janisková, M., Keeley, S., Laloyaux, P., Lopez, P., Lupu, C., Radnoti, G., Rosnay, P., Rozum, I., Vamborg, F., Villaume, S., Thépaut, J.N., 2020. The ERA5 global reanalysis. Quarterly Journal of the Royal Meteorological Society 146, 1999–2049. URL: https://doi.org/10.1002/qj.3803, doi:10.1002/qj.3803.

Jain, S., 2007. An Empirical Economic Assessment of Impacts of Climate Change on Agriculture in Zambia. Policy Research

Working Paper 4291. World Bank. Washington, DC. URL: http://hdl.handle.net/10986/7478. license: CC BY 3.0 IGO.

Kaczan, D., Arslan, A., Lipper, L., 2013. Climate-Smart Agriculture? A review of current practice of agroforestry and conservation agriculture in Malawi and Zambia. Working or Discussion Paper 13-07. Food and Agriculture Organization of the United Nations (FAO). URL: https://ageconsearch.umn.edu/record/288985, doi:10.22004/ag.econ.288985. fAO Document Repository: http://www.fao.org/3/a-ar715e.pdf.

Katiraie-Boroujerdy, P.S., Rahnamay Naeini, M., Akbari Asanjan, A., Chavoshian, A., Hsu, K.l., Sorooshian, S., 2020. Bias correction of satellite-based precipitation estimations using quantile mapping approach in different climate regions of iran. Remote Sensing 12, 2102. URL: http://dx.doi.org/10.3390/rs12132102, doi:10.3390/rs12132102.

Lakew, H.B., 2020. Investigating the effectiveness of bias correction and merging mswep with gauged rainfall for the hydrological simulation of the upper blue nile basin. Journal of Hydrology: Regional Studies 32, 100741. URL: https://www.sciencedirect.com/science/article/pii/S2214581820302159, doi:https://doi.org/10.1016/j.ejrh.2020.100741.

Le, X.H., Nguyen Van, L., Hai Nguyen, D., Nguyen, G.V., Jung, S., Lee, G., 2023. Comparison of bias-corrected multisatellite precipitation products by deep learning framework. International Journal of Applied Earth Observation and Geoinformation 116, 103177. URL: http://dx.doi.org/10.1016/j.jag.2022.103177, doi:10.1016/j.jag.2022.103177.

Li, X., Chen, Y., Zhang, Y., Chen, L., 2023. Bias adjustment of satellite rainfall data through gaussian process regression (gpr) based on rain intensity classification in the greater bay area, china. Theoretical and Applied Climatology 152, 1115–1127. URL: http://dx.doi.org/10.1007/s00704-023-04435-y, doi:10.1007/s00704-023-04435-y.

Lober, C., Fayne, J., Hashemi, H., Smith, L.C., 2023. Bias correction of 20 years of imerg satellite precipitation data over canada

and alaska. Journal of Hydrology: Regional Studies 47, 101386. URL: https://www.sciencedirect.com/science/article/pii/S2214581823000733, doi:https://doi.org/10.1016/j.ejrh.2023.101386.

Maidment, R.I., Grimes, D., Black, E., Tarnavsky, E., Young, M., Greatrex, H., Allan, R.P., Stein, T., Nkonde, E., Senkunda, S., Alcántara, E.M.U., 2017. A new, long-term daily satellite-based rainfall dataset for operational monitoring in africa. Scientific Data 4. URL: https://doi.org/10.1038/sdata.2017.63, doi:10.1038/sdata.2017.63.

Maphugwi, M., Blamey, R.C., Reason, C.J., 2024. Rainfall characteristics over the congo air boundary region in southern africa: A comparison of station and gridded rainfall products. Atmospheric Research 311, 107718. URL: https://www.sciencedirect.com/science/article/pii/S0169809524005003, doi:https://doi.org/10.1016/j.atmosres.2024.107718.

Maraun, D., 2013. Bias correction, quantile mapping, and downscaling: Revisiting the inflation issue. Journal of Climate 26, 2137–2143. URL: http://dx.doi.org/10.1175/JCLI-D-12-00821.1, doi:10.1175/jcli-d-12-00821.1.

Mekonnen, K., Velpuri, N.M., Leh, M., Akpoti, K., Owusu, A., Tinonetsana, P., Hamouda, T., Ghansah, B., Paranamana, T.P., Munzimi, Y., 2023. Accuracy of satellite and reanalysis rainfall estimates over africa: A multi-scale assessment of eight products for continental applications. Journal of Hydrology: Regional Studies 49, 101514. URL: http://dx.doi.org/10.1016/j.ejrh.2023.101514, doi:10.1016/j.ejrh.2023.101514.

Mendez, M., Maathuis, B., Hein-Griggs, D., Alvarado-Gamboa, L.F., 2020. Performance evaluation of bias correction methods for climate change monthly precipitation projections over costa rica. Water 12, 482. URL: http://dx.doi.org/10.3390/w12020482, doi:10.3390/w12020482.

Nigussie, A.B., Tenfie, H.W., Zimale, F.A., Endalew, A., Wudiye, G., 2022. Evaluation of multiple bias correction methods with different satellite rainfall products in the main beles watershed, upper blue nile (abbay) basin, ethiopia. Journal of Water and Climate Change 14, 156–174. URL: http://dx.doi.org/10.2166/wcc.2022.244, doi:10.2166/wcc.2022.244.

Oduro, C., Bi, S., Wu, N., Agyemang, S., Baidu, M., Babaousmail, H., Iyakaremye, V., Nnamdi Dike, V., Odhiambo Ayugi, B., 2024. Estimating surface air temperature from multiple gridded observations and reanalysis datasets over ghana. Advances in Space Research 73, 537–552. URL: http://dx.doi.org/10.1016/j.asr.2023.10.029, doi:10.1016/j.asr.2023.10.029.

Rasmussen, C.E., Williams, C.K.I., 2006. Gaussian Processes for Machine Learning. MIT Press. URL: https://gaussianprocess.org/gpml/.

Schmidli, J., Frei, C., Vidale, P.L., 2006. Downscaling from GCM precipitation: a benchmark for dynamical and statistical downscaling methods. International Journal of Climatology 26, 679–689. URL: https://doi.org/10.1002/joc.1287, doi:10.1002/joc.1287.

Schulz, E., Speekenbrink, M., Krause, A., 2018. A tutorial on gaussian process regression: Modelling, exploring, and exploiting functions. Journal of Mathematical Psychology 85, 1–16. URL: http://dx.doi.org/10.1016/j.jmp.2018.03.001, doi:10.1016/j.jmp.2018.03.001.

Schölkopf, B., Smola, A.J., Williamson, R.C., Bartlett, P.L., 2000. New support vector algorithms. Neural Computation 12, 1207–1245. URL: https://doi.org/10.1162/089976600300015565, doi:10.1162/089976600300015565, arXiv:https://direct.mit.edu/neco/article-pdf/12/5/1

Shen, Z., Yong, B., Gourley, J.J., Qi, W., 2021. Real-time bias adjustment for satellite-based precipitation estimates over mainland china. Journal of Hydrology 596, 126133. URL: http://dx.doi.org/10.1016/j.jhydrol.2021.126133, doi:10.1016/j.jhydrol.2021.126133.

Soo, E.Z.X., Jaafar, W.Z.W., Lai, S.H., Othman, F., Elshafie, A., Islam, T., Srivastava, P., Hadi, H.S.O., 2019. Evaluation of bias-adjusted satellite precipitation estimations for extreme flood events in langat river basin, malaysia. Hydrology Research 51, 105–126. URL: http://dx.doi.org/10.2166/nh.2019.071, doi:10.2166/nh.2019.071.

STERN, R.D., COOPER, P.J.M., 2011. ASSESSING CLIMATE RISK AND CLIMATE CHANGE USING RAINFALL DATA –

a CASE STUDY FROM ZAMBIA. Experimental Agriculture 47, 241–266. URL: https://doi.org/10.1017/s0014479711000081, doi:10.1017/s0014479711000081.

Tao, Y., Gao, X., Hsu, K., Sorooshian, S., Ihler, A., 2016. A deep neural network modeling framework to reduce bias in satellite precipitation products. Journal of Hydrometeorology 17, 931 – 945. doi:10.1175/JHM-D-15-0075.1.

Tarnavsky, E., Grimes, D., Maidment, R., Black, E., Allan, R.P., Stringer, M., Chadwick, R., Kayitakire, F., 2014. Extension of the tamsat satellite-based rainfall monitoring over africa and from 1983 to present. Journal of Applied Meteorology and Climatology 53, 2805–2822. URL: http://dx.doi.org/10.1175/JAMC-D-14-0016.1, doi:10.1175/jamc-d-14-0016.1.

Torgbor, F.F., Stern, D., Nkansah, B.K., Stern, R., 2018. Rainfall modelling with a transect view in ghana. Ghana Journal of Science 58, 41–57.

Toté, C., Patricio, D., Boogaard, H., Van der Wijngaart, R., Tarnavsky, E., Funk, C., 2015. Evaluation of satellite rainfall estimates for drought and flood monitoring in mozambique. Remote Sensing 7, 1758–1776. URL: http://dx.doi.org/10.3390/rs70201758, doi:10.3390/rs70201758.

Tripathi, S., Srinivas, V., Nanjundiah, R.S., 2006. Downscaling of precipitation for climate change scenarios: A support vector machine approach. Journal of Hydrology 330, 621–640. URL: https://www.sciencedirect.com/science/article/pii/S0022169406002368, doi:https://doi.org/10.1016/j.jhydrol.2006.04.030.

Waongo, M., Garba, J.N., Diasso, U.J., Sawadogo, W., Sawadogo, W.L., Daho, T., 2024. A merging approach for improving the quality of gridded precipitation datasets over burkina faso. Climate 12. URL: https://www.mdpi.com/2225-1154/12/12/226, doi:10.3390/cli12120226.

Yang, X., Yong, B., Hong, Y., Chen, S., Zhang, X., 2016. Error analysis of multi-satellite precipitation estimates with an independent raingauge observation network over a medium-sized humid basin. Hydrological Sciences Journal ,

1–18URL: http://dx.doi.org/10.1080/02626667.2015.1040020, doi:10.1080/02626667.2015.1040020.

Yang, Z., Villarini, G., 2019. Examining the capability of reanalyses in capturing the temporal clustering of heavy precipitation across europe. Climate Dynamics 53, 1845–1857. URL: http://dx.doi.org/10.1007/s00382-019-04742-z, doi:10.1007/s00382-019-04742-z.

Zambrano-Bigiarini, M., Nauditt, A., Birkel, C., Verbist, K., Ribbe, L., 2017. Temporal and spatial evaluation of satellite-based rainfall estimates across the complex topographical and climatic gradients of chile. Hydrology and Earth System Sciences 21, 1295–1320. URL: http://dx.doi.org/10.5194/hess-21-1295-2017, doi:10.5194/hess-21-1295-2017.

Zhang, L., Xin, Z., Zhang, C., Song, C., Zhou, H., 2022. Exploring the potential of satellite precipitation after bias correction in streamflow simulation in a semi-arid watershed in northeastern china. Journal of Hydrology: Regional Studies 43, 101192. URL: https://www.sciencedirect.com/science/article/pii/S2214581822002051, doi:https://doi.org/10.1016/j.ejrh.2022.101192.